Platform for micro-invasive membrane-free biochemical sampling of brain interstitial fluid

ENGINEERING

Platform for micro-invasive membrane-free biochemical sampling of brain interstitial fluid

Ritu Raman[1]*, Erin B. Rousseau[1,2]*, Michael Wade[1], Allison Tong[1], Max J. Cotler[1,2], Jenevieve Kuang[1,3], Alejandro Aponte Lugo[1], Elizabeth Zhang[1,4], Ann M. Graybiel[4,5], Forest M. White[1,3,6], Robert Langer[1,7], Michael J. Cima[1,8†]

Neurochemical dysregulation underlies many pathologies and can be monitored by measuring the composition of brain interstitial fluid (ISF). Existing in vivo tools for sampling ISF do not enable measuring large rare molecules, such as proteins and neuropeptides, and thus cannot generate a complete picture of the neurochemical connectome. Our micro-invasive platform, composed of a nanofluidic pump coupled to a membrane-free probe, enables sampling multiple neural biomarkers in parallel. This platform outperforms the state of the art in low-flow pumps by offering low volume control (single stroke volumes, <3 nl) and bidirectional fluid flow (<100 nl/min) with negligible dead volume (<30 nl) and has been validated in vitro, ex vivo, and in vivo in rodents. ISF samples (<1.5 μL) can be processed via liquid chromatography–tandem mass spectrometry. These label-free liquid biopsies of the brain could yield a deeper understanding of the onset, mechanism, and progression of diverse neural pathologies.

INTRODUCTION

Neural pathology is characterized by electrical and chemical dysregulation in distinct brain circuits, and a range of techniques has been developed for studying these signals in vivo in physiological and pathological states (*1*, *2*). Tools for measuring and modulating electrical signaling, such as implanted microelectrodes, have generated a deeper understanding of neural network dynamics (*3*–*6*). They do not, however, fully represent the complexity of in vivo signaling because they only sense redox-active analytes. Existing tools thus cannot form a spatial and neuroanatomical map of the complete neurochemical connectome, the neurochemicals in the brain underlying processing of motoric, sensory, and cognitive information (*7*). Techniques such as microdialysis, cell-based biosensors, and aptamer-functionalized field-effect transistors overcome this limitation by enabling in vivo sampling of electroneutral neurochemicals (*8*–*10*). These tools have provided valuable insight into the in vivo composition, concentration, and distribution of small and widely prevalent neurotransmitters such as γ-aminobutyric acid (GABA), glutamate, acetylcholine, and serotonin. The missing piece in mapping the neurochemical connectome is a tool for micro-invasively monitoring larger rarer neurochemicals, such as neuropeptides and proteins (*11*–*14*).

Adapting the most commonly used neurochemical sampling method, microdialysis, to suit this application is impractical and undesirable for a few reasons. Microdialysis relies on collecting neurochemicals from interstitial fluid (ISF) via diffusion across a semipermeable membrane (*8*, *15*, *16*). Extraction loss across the semipermeable membrane limits the measurable concentration of neurochemicals from interstitial space (*8*). Recovery fractions can be improved by decreasing flow rate, but this increases sampling time, thereby decreasing the total mass of neurochemicals collected and the total sample volume collected. Increasing membrane length can also enhance recovery fraction, but this reduces the spatial resolution of sampling from a specific neural node. The large size of certain neurochemicals such as neuropeptides and proteins, and their proclivity for nonspecific absorption to membranes, motivates increasing membrane pore size, but this can result in leakage of perfusion liquid into the surrounding tissue (*17*–*19*). Membranes also remove the capacity to measure the contents of dense core extracellular vesicles, which carry proteins and nucleic acids and play an important role in cell-cell signaling in the brain (*20*). The large sizes of microdialysis probes (150 to 400 μm), moreover, limit spatial resolution and damage delicate brain architecture, leading to probe failure due to tissue scarring and making the technique incompatible with longitudinal studies of the neurochemical connectome (*19*, *21*, *22*). Micro-invasive and membrane-free in vivo sampling of large rare neural biomarkers in ISF in parallel is, therefore, a critical unmet need in neuroscience (*17*). Addressing this need will require developing a sampling platform that can extract small volumes of ISF from the brain using a micro-invasive probe that does not require a membrane. We have designed a platform that matches these requirements and demonstrate its ability to perform acute sampling of large neural proteins in vivo.

RESULTS

Design and manufacture of nitinol-activated nanofluidic pump

We have constructed a micro-invasive membrane-free sampling platform for directly extracting small volumes of ISF from distinct neural nodes and demonstrated the ability to identify and quantify a wide range of neurochemicals within extracted samples. The platform is composed of a custom nanofluidic peristaltic pump

[1]Koch Institute for Integrative Cancer Research, Massachusetts Institute of Technology, Cambridge, MA, USA. [2]Harvard-MIT Program in Health Sciences and Technology, Massachusetts Institute of Technology, Cambridge, MA, USA. [3]Center for Precision Cancer Medicine, Massachusetts Institute of Technology, Cambridge, MA, USA. [4]McGovern Institute for Brain Research, Massachusetts Institute of Technology, Cambridge, MA, USA. [5]Department of Brain and Cognitive Sciences, Massachusetts Institute of Technology, Cambridge, MA, USA. [6]Department of Biological Engineering, Massachusetts Institute of Technology, Cambridge, MA, USA. [7]Department of Chemical Engineering, Massachusetts Institute of Technology, Cambridge, MA, USA. [8]Department of Materials Science and Engineering, Massachusetts Institute of Technology, Cambridge, MA, USA.
*These authors contributed equally to this work.
†Corresponding author. Email: mjcima@mit.edu

(nanopump) coupled to a micro-invasive membrane-free probe. The nanopump is composed of heat-sensitive wires, made of the shape memory alloy nitinol, and wrapped around custom-manufactured styrene ethylene butylene styrene (SEBS) tubing (Fig. 1A). The wires undergo a phase transition when heated to 70°C, accomplished by passing a current through the wire and driving ohmic heating as a result of the alloy's high electrical resistance. Heating results in physical contraction of the wires up to 5% of their original length and displaces fluid within the SEBS tube. Removal of the current results in cooling that relaxes the wire and tubing. Sequential contraction of the nitinol actuators drives peristaltic fluid flow, with flow direction dependent on the sequence of wire contraction.

The nanopump's flow rate can be tuned via a range of design parameters. Initial studies with commercially purchased SEBS tubing (1 mm outer diameter, 0.5 mm inner diameter) demonstrated directional flow control (Fig. 1B), but resultant flow rates were too fast to be used inside the brain, which requires flow rates <100 nl/min (*3*). The efficiency of the flow cycle was also mitigated by backflow in the tubing between subsequent pumping cycles, as this reduced the net volume of directional fluid flow per cycle. Several parameters control nanopump performance including actuator time on, actuator time off, overlap time between actuators, and overlap time between cycles. These parameters were optimized to choose the highest flow rate, indicating a more efficient flow cycle with reduced backflow (fig. S1). Nitinol wire pre-tension was also shown to affect nanopump performance. Pre-tension was defined as the degree to which the tube was compressed when an individual nitinol wire was in its uncontracted state. Wires with a pre-tension of 0% shifted along the length of the tubing during contraction and cooling, reducing the efficiency and reproducibility of fluid flow and increasing backflow. Much higher degrees of pre-tension constrict the

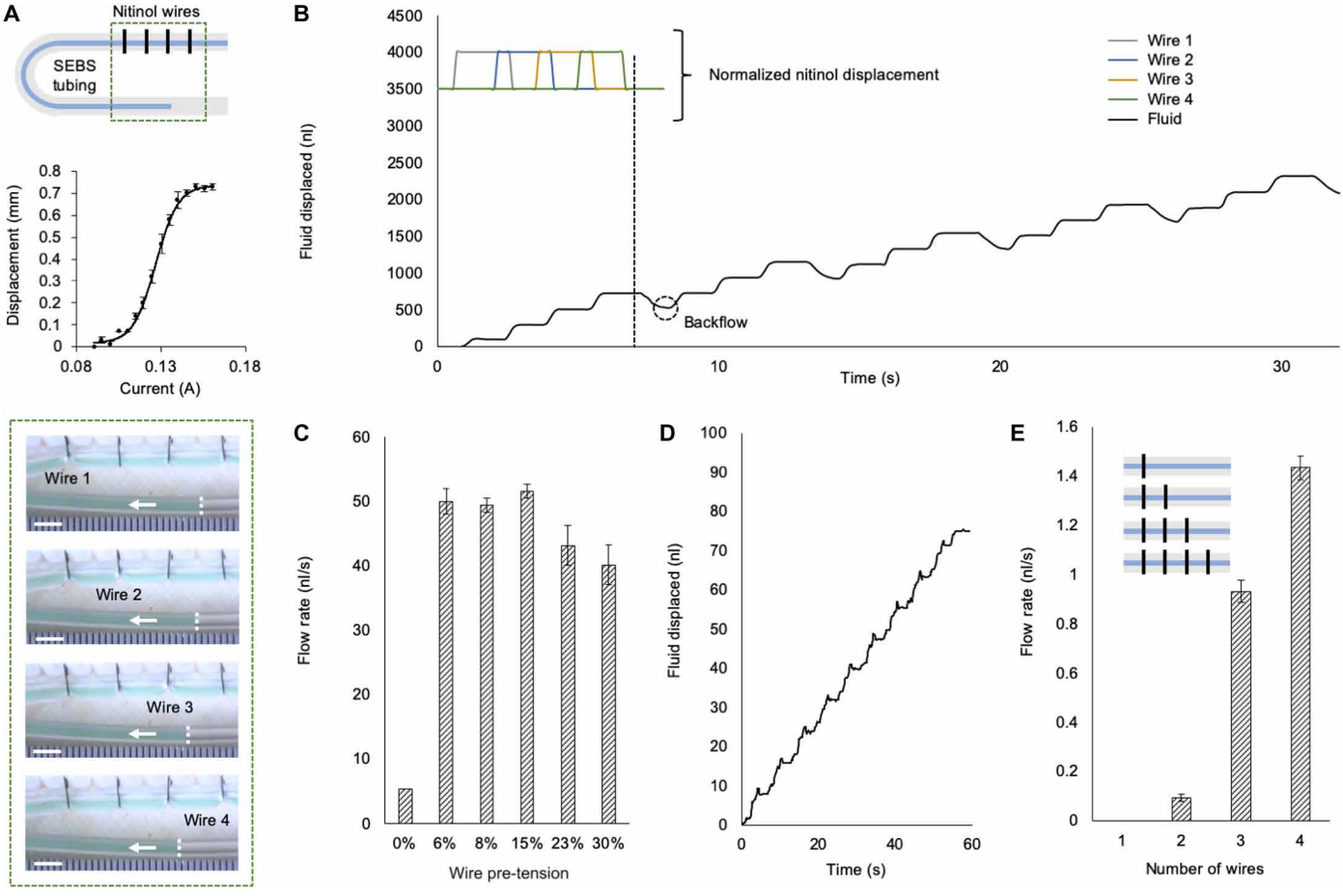

Fig. 1. Design and characterization of a nitinol-activated nanofluidic pump. (**A**) Top: Schematic of nitinol wire–driven peristaltic pumping. Middle: Deformation of tubing (1 mm outer diameter, 0.5 mm inner diameter) in response to nitinol wire contraction ($n = 3$). Wire length = 14.6 mm. Wire diameter = 100 μm. Bottom: Images of nitinol wire–driven peristaltic pumping. Flow in one direction is driven by sequential contraction of wires in that direction. Scale bars, 2 mm. (**B**) Fluid displaced as a function of time in response to sequential wire contraction with 500-ms overlap between wires. Lack of overlap between the fourth and first wires between cycles results in backflow. (**C**) Fluid flow rate is influenced by wire pre-tension ($n = 3$), the percentage of its original width to which the tubing is compressed. Small values of pre-tension ensure that the wires do not slide along the tubing between contraction-relaxation cycles, increasing flow efficiency, while large values of pre-tension constrict the tube lumen and reduce flow rate. (**D**) Fluid flow rate is reduced to values commensurate with in vivo use (75.9 nl/min, 1.5 nl of backflow per pumping cycle) by using a custom-manufactured tubing (1 mm outer diameter, 0.1 mm inner diameter). (**E**) Fluid flow efficiency increases with increasing number of actuator wires, with flow rates and SDs matching our design requirements for flow driven by four wires ($n = 3$).

inner channel of the tubing, reducing fluid stroke volume in response to actuator contraction and thereby decreasing the resultant flow rate. Pre-tensions between 5 and 15% were shown to maximize flow efficiency (Fig. 1C). Custom-manufactured SEBS tubing of reduced inner diameter (100 μm) was manufactured to enable more precise nanofluidic control and target the lower flow rates required for in vivo applications. This reduced directional flow rates to values commensurate with testing in brain tissue and resulted in negligible backflow (Fig. 1D). Varying the number of actuator wires confirmed that flow rates of around 50 to 100 nl/min (0.83 to 1.7 nl/s) could be achieved with three or more wires (Fig. 1E). Pumps operating with four wires were used for all following experiments.

A single lumen borosilicate capillary (80 μm outer diameter, 50 μm inner diameter) is inserted directly into the pump tubing (1 mm outer diameter, 100 μm inner diameter) without interfacing connectors, as required for traditional syringe pumps, thus drastically reducing pump dead volume to <30 nl, as compared to ~1 to 3 μl for syringe-based systems. These micro-invasive probes can be directly inserted and steered within the brain and demonstrate significantly less chronic glial scarring after 8 weeks as compared to larger diameter devices (≥150 μm) (*23*). Small lumens of this size, moreover, prevent the entry of large debris and do not clog (*24*). This removes the need for a membrane when the probes are implanted long term. The nanopump can drive fluid in both infusion and sampling modes through the probes, with similar flow rates in both directions (Fig. 2, A and B). Flow rate is determined by the inner diameter of the probe with increasing diameters corresponding to increasing flow rates (Fig. 2C). The nanofluidic sampling platform retains functionality in agarose gel brain phantoms, which are commonly used for in vitro characterization of neural implants as they mimic the mechanical properties of brain tissue (*3*, *9*, *23*). Push-pull perfusion performed in agarose gels demonstrated that infusing blue dye into yellow-dyed gels resulted in extracting green-dyed samples, generated by fluid mixing between the blue and yellow dyes (Fig. 2, D and E, and fig. S2). The sampling flow rate in agarose gels is lower than the infusion flow rate for the same flow control parameters, and this behavior is attributed to the fluidic resistance generated by the hydrogel as compared to air. Fluid flow rates <100 nl/min were targeted, as these have previously been deemed safe for in vivo use (*3*).

This simple two-component pump and probe design enables low-flow push-pull perfusion from a single lumen with negligible dead volume, providing a significant advantage over previous neurochemical sampling techniques that rely on significantly larger dual-lumen probes coupled to syringe-based pumps with microliter dead volumes (*25*, *26*). The nanofluidic sampling platform offers improved safety and efficacy as compared to these platforms because it reduces the size of the inserted probes and the volume of ISF that must be sampled to perform a liquid biopsy of the brain.

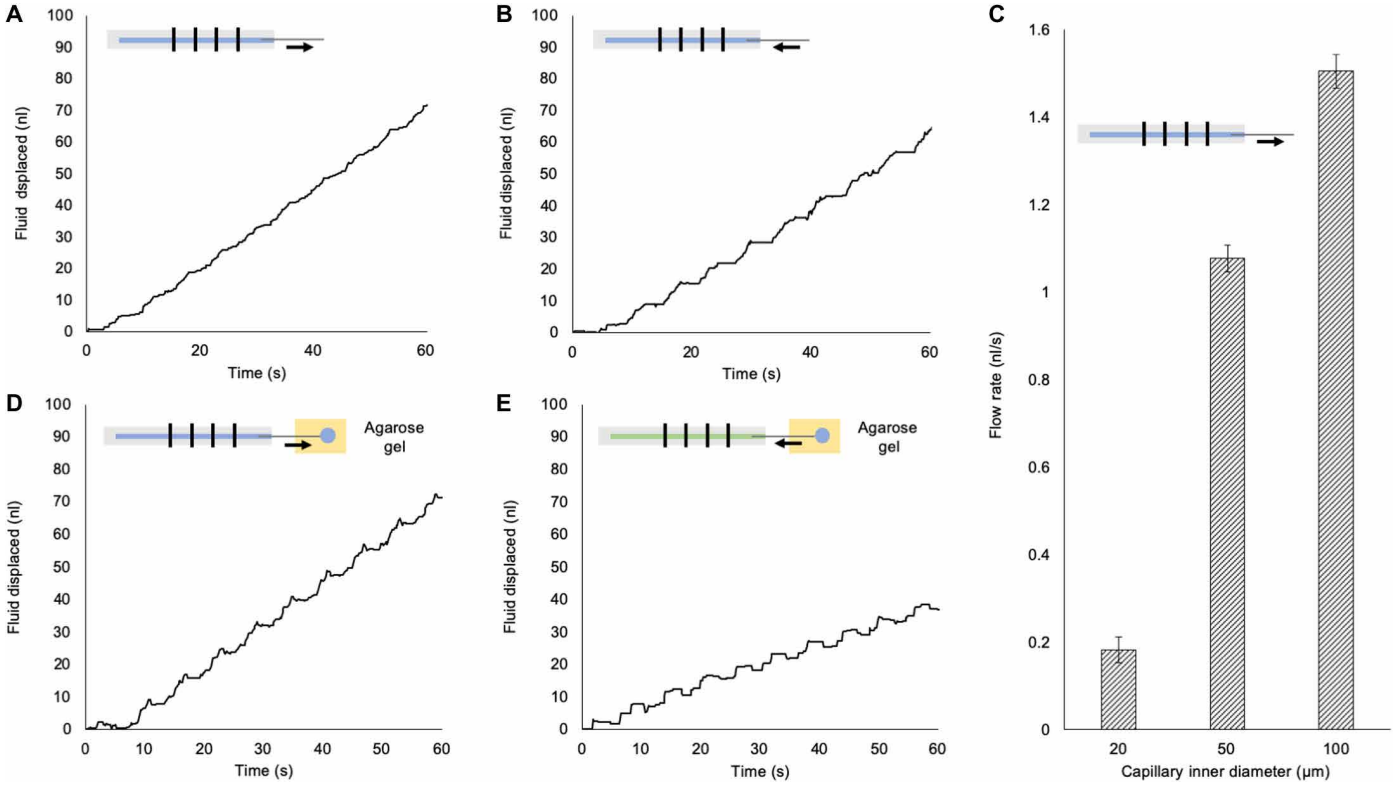

Fig. 2. Nanopump-driven infusion and sampling through a micro-invasive neural probe. (**A**) Fluid displacement tracking of nanopump-driven infusion through a borosilicate capillary (80 μm outer diameter, 50 μm inner diameter). (**B**) Fluid displacement tracking of nanopump-driven sampling through a borosilicate capillary (80 μm outer diameter, 50 μm inner diameter). (**C**) Infusion flow rate as a function of borosilicate capillary inner diameter ($n = 3$ per group). (**D**) Fluid displacement tracking of nanopump-driven infusion through a borosilicate capillary (80 μm outer diameter, 50 μm inner diameter) into an agarose gel brain phantom. (**E**) Fluid displacement tracking of nanopump-driven sampling through a borosilicate capillary (80 μm outer diameter, 50 μm inner diameter) from an agarose gel brain phantom. Sampling was performed after infusion.

The novel pump design also offers both precise low-volume control (single stroke volumes, <3 nl) and bidirectional fluid flow, capabilities not demonstrated by other low-flow pumps controlled by either nitinol or other actuators (*27*–*30*). These advantages over the state-of-the-art motivated, further optimizing the sampling platform for in vivo use.

Miniaturization, optimization, and benchmarking of nanofluidic sampling platform

The benchtop prototype of our nanopump was reduced to a portable size for in vivo use by powering the wires with a battery and controlling their sequential contraction with a microcontroller (Fig. 3A and fig. S3). Pump power consumption and battery run time were characterized as a function of wire diameter and length (fig. S4). This confirmed that neither battery run time nor fatigue-induced wire fracture was a limiting factor for in vivo experiments, as they far exceeded the estimated required sampling time (≤30 min).

Fluid flow rate and variability across trials are a function of whether the tubing under the wire is filled with liquid, with more consistent results observed in filled tubes (Fig. 3B). Overlap time between sequential wire contraction was varied to identify effect on

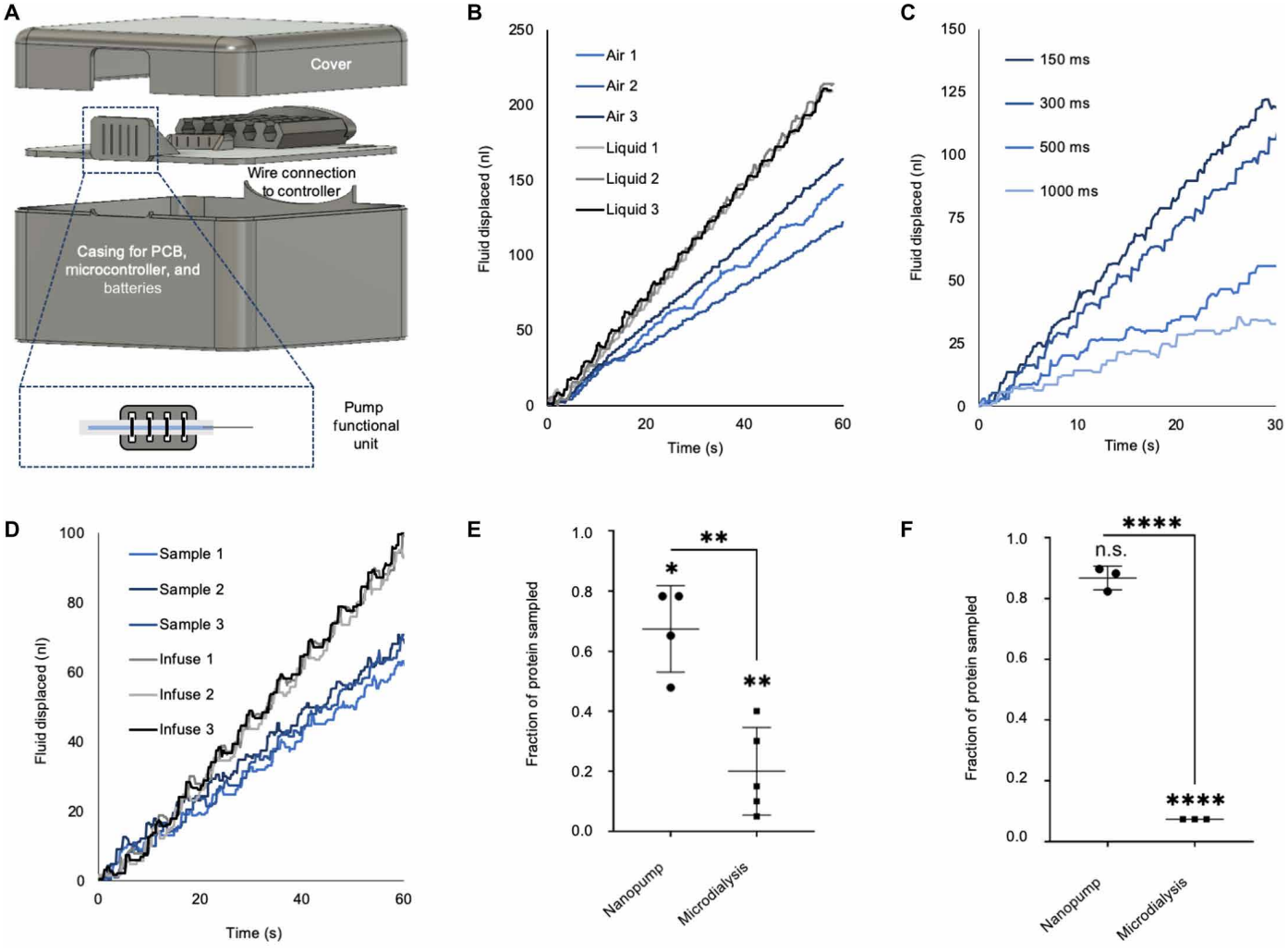

Fig. 3. Miniaturization, optimization, and benchmarking of nanofluidic sampling platform. (**A**) Schematic of portable nanopump design, converting the benchtop prototype into a handheld battery-powered device, thereby enabling in vivo use. Photograph of manufactured portable nanopump in fig. S3. PCB, printed circuit board. (**B**) Fluid displaced as a function of time is a function of whether the nitinol wires operate on tubing filled with ambient air (trials 1, 2, and 3) or water (trials 1, 2, and 3). (**C**) Fluid displaced as a function of time for differing degrees of overlap (150 to 1000 ms) between wires during sequential contraction. (**D**) Fluid displaced as a function of time for optimized flow control code during infusion through and sampling from a borosilicate capillary (80 μm outer diameter, 50 μm inner diameter). Data from three separate trials are presented for both infusion and sampling. (**E**) MBP (~13 to 21 kDa) content in samples extracted using nanopump platform and standard microdialysis platform and compared to a control of known concentration. The nanopump-extracted sample significantly outperforms microdialysis in the measurement of this molecule, as it avoids sample extraction loss across a membrane. Samples were measured using a spectrophotometer. * represents analysis of variance (ANOVA) post hoc Tukey test, $P \leq 0.05$. ** represents ANOVA post hoc Tukey test, $P \leq 0.01$. (**F**) Hemoglobin (~64.5 kDa) content in samples extracted using nanopump platform and standard microdialysis platform and compared to a control of known concentration. The nanopump-extracted sample is not significantly different from the control and significantly outperforms microdialysis in the measurement of this molecule, as it avoids sample extraction loss across a membrane. n.s. represents ANOVA post hoc Tukey test $P > 0.05$. **** represents ANOVA post hoc Tukey test $P \leq 0.0001$.

flow rate, and a flow control code that maintained both infusion and sampling rates below 100 nl/min was chosen for subsequent experiments (Fig. 3, C and D). Flow rate consistency between trials served as validation that performance in vivo would likely be maintained within a tightly controlled and predetermined range.

Elevation of the probe relative to the nitinol actuators resulted in no observable difference in flow rate, indicating that the pump could reliably pump against a height gradient (fig. S5A). Increasing the distance between the probe and the nitinol actuators also did not significantly affect flow rate, but as longer distances appeared to increase flow rate variation across trials, distances ≤100 mm were used in subsequent experiments (fig. S5B). Previous demonstrations have shown that probes can be implanted chronically in rodent brains and retain fluidic functionality up to 1 year after implantation (*24*). To test whether the pump could be readily detached from and reattached to a chronically implanted probe, we engineered a removable connector, composed of a 30-gauge (G) needle bonded to a polyether ether ketone (PEEK) tubing. This connector retained fluidic functionality while decreasing flow rate through the probe, but this can be readily tuned by altering the wire overlap time (fig. S5C). The connector could be used, in the future, for chronic ISF sample collection from a single location in the brain through an implanted probe by simply attaching and detaching the nanopump at different time points (fig. S5D).

An in vitro comparison of the membrane-free platform and a standard microdialysis setup was performed by using both tools to measure fluidic samples of known chemical concentration and composition. Time-matched samples from a push-pull perfusion (10-min infusion, 20-min withdrawal) conducted with the nanopump-driven platform, as well as samples collected from a 30-min microdialysis perfusion, were analyzed for total protein content using either a spectrophotometer or via liquid chromatography–tandem mass spectrometry (LC-MS/MS). Both sampling techniques demonstrated similar abilities to accurately sample substance P (1347.63 Da), as compared to each other and a control (fig. S5E). The nanopump platform significantly outperformed microdialysis, however, in its ability to measure the larger molecules myelin basic protein (MBP; ~13 to 21 kDa) and hemoglobin (64,458 Da) (Fig. 3, E and F). It demonstrated minimal extraction loss of MBP, measuring average sample concentrations of 67.4% of the control stock solution, as opposed to microdialysis, which only measured 20.0% of the control. Similarly, the nanopump demonstrated minimal extraction loss of hemoglobin, measuring average sample concentrations of 86.8% of the control stock solution, as opposed to microdialysis, which only measured 7.3% of the control. This confirmed the hypothesis that this micro-invasive membrane-free tool is uniquely suited to the measurement of large rare neurochemicals, as it limits the extraction loss of these biomarkers across membranes.

Ex vivo characterization of nanofluidic sampling platform

The nanofluidic platform can be used to infuse fluid into and sample fluid from ex vivo brain tissue in addition to agarose gel brain phantoms. The sampling platform can be directly interfaced with brain regions of interest via the borosilicate probe without the use of a guide tube (Fig. 4, A and B). This enables fluidic delivery with less damage to surrounding tissues by reducing the device's spatial footprint (*23*). The pump's ability to deliver small volumes at infusion rates below the safety threshold of 100 nl/min to ex vivo rat brain tissue was evaluated. The borosilicate probes were lowered 5 mm from the dorsal surface of an ex vivo brain to target deep structures. Dye was loaded into the nanopump and infused through the probes into an ex vivo brain for 1 min at 95 nl/min. Histology demonstrated successful bolus delivery into the brain (Fig. 4C). A fluorescent dye infused for 30 s into the right hemisphere and 60 s into the left hemisphere of an ex vivo brain, imaged using a fluorescent In Vivo Imaging System (IVIS), demonstrated a proportional increase in bolus size (as quantified by radiant efficiency), with increased delivery time (Fig. 4D). A series of fluorescent images were obtained every 6 s during a continuous infusion to better characterize this relationship, demonstrating that radiant efficiency increased linearly with infusion time (Fig. 4E and fig. S6B). This corroborated the results obtained with preceding agarose gel infusion studies. These results validate the platform's ability to perform consistent low-volume infusion to deep brain structures at low flow rates.

In vivo characterization of nanofluidic sampling platform

The sampling modality of the system was characterized acutely in vivo. Following craniotomy, a probe directly interfaced with the pump was implanted to target the rat substantia nigra (fig. S6C). Artificial cerebrospinal fluid (aCSF) was infused into the tissue for 10 min (95 nl/min) followed by a 20-min withdraw period (65 nl/min). Sampled ISF was analyzed via LC-MS/MS. Processing protocols were optimized for proteomics rather than small-molecule detection. Following a trypsin digest, proteins abundant in the rat brain were identified to demonstrate proof of ISF sampling.

A total of 96 proteins were identified in our first in vivo sample. Proteins were identified using a MS software search engine (Mascot) that uses an algorithm to assess the probability of an MS/MS spectrum matching to a given peptide from a database. Among the identified proteins, MBP (~13 to 21 kDa), brain acid soluble protein-1 (BASP-1; ~22 kDa), and γ-enolase (~39 kDa) were of particular interest (Fig. 5), as they are known to be observed in healthy CSF, and their concentrations change during instances of neurologic disease (*31*, *32*). Previously used tools to quantify biochemicals in neural ISF have generated insights on much smaller molecules by comparison, such as GABA (~100 Da), glutamate (~150 Da), acetylcholine (~150 Da), and serotonin (~180 Da). These results thus demonstrate the superior ability of our micro-invasive platform to sample proteins as trackable biomarkers in the brain in vivo. Adjusting sampling time and developing robust optimized protein isolation protocols will allow for collection and detection of less abundant proteins and peptides in future work (fig. S6D).

Performing nanopump-driven in vivo ISF sampling from the substantia nigra in two additional rats revealed that this method was robust and repeatable. Of the 136 peptides identified, 77 (56.7% of total) overlapped with another biological replicate, while 28 (20.6% of total) were detected in all replicates (Fig. 6 and table S1). Among the proteins identified in all three samples were transthyretin (~14 kDa), believed to be produced in the choroid plexus and observed in higher levels in brain tissue and CSF, and kinesin-like protein 15 (~160 kDa), a motor enzyme most associated with axon growth and maintenance (*33*, *34*). Variance among the proteins sampled from biological replicates could be accounted for by data-dependent MS analysis and brain heterogeneity. Variability in transcription, translation, and protein expression between brain regions and cell types is well documented (*35*, *36*). Minute differences in probe placement in relation to an animal's unique

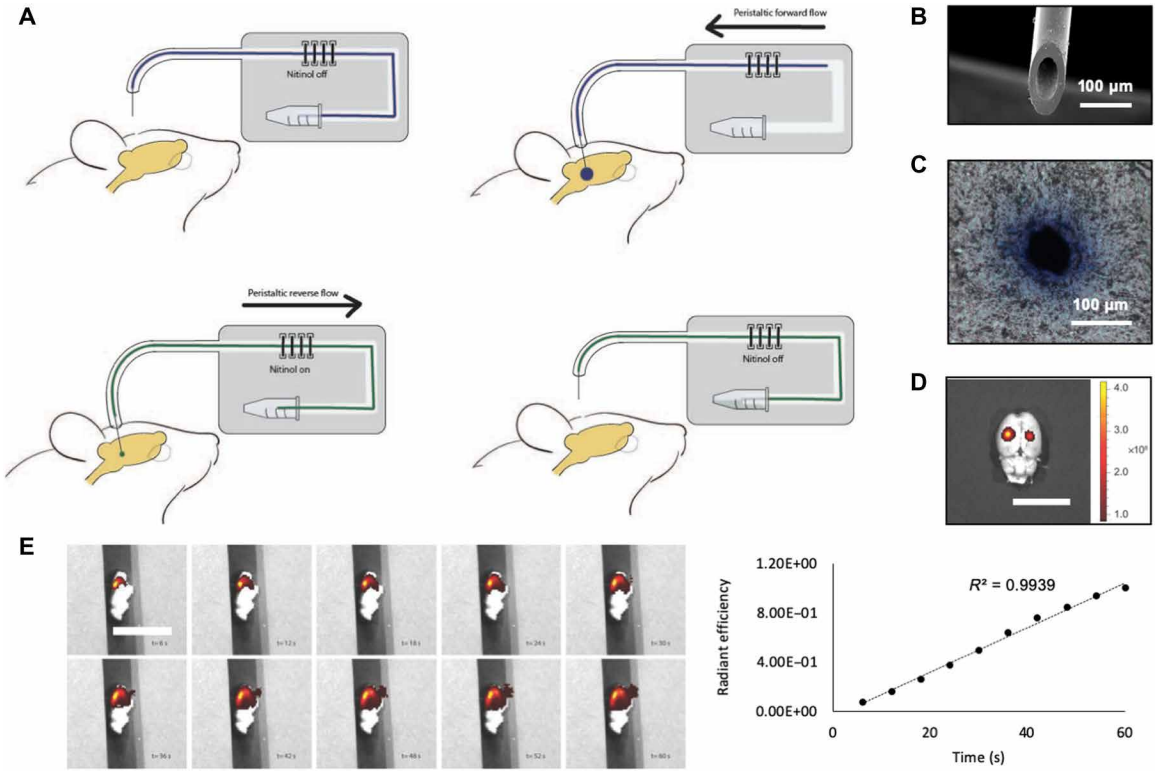

Fig. 4. Ex vivo characterization of nanofluidic sampling platform. (**A**) Schematic of sampling platform interfacing with rodent brain to collect samples of ISF. This methodology could potentially be adapted for chronic sampling (fig. S5D). (**B**) Scanning electron microscope image of borosilicate capillary. (**C**) Histological slice of rodent brain showing infusion of trypan blue into ex vivo tissue. (**D**) Fluorescent imaging of ex vivo brain showing a Genhance 750 dye bolus volume control as a function of infusion time (30 s right hemisphere, 60 s left hemisphere). Scale bar, 2 cm. (**E**) Time-lapse imaging (left) of fluorescent dye bolus volume in ex vivo brain showing linear increase (right) in volume as a function of infusion time. Scale bar, 2 cm. Data from two additional infusions are shown in fig. S6B.

physiology could position the probe near different cells, affecting the contents of small volumes of ISF captured by the sampling platform. Variance introduced through surgery, moreover, including trauma associated with probe placement, can also explain sample heterogeneity.

DISCUSSION

Neurological disorders are characterized by electrical and biochemical dysregulation in specific brain regions. Existing tools to dynamically characterize biochemical dysregulation in vivo do not enable quantitative and parallel identification of all biomarkers present within ISF, particularly long-chain rare neurochemicals and the contents of dense core extracellular vesicles. Tracking these molecules requires sacrificing subjects from animal models of disease and conducting immunohistochemical staining on tissue slices. These techniques are often nonspecific and rely on terminal surgical procedures and are thus unable to track the dynamic fluctuations of large rare neurochemicals over time in a single animal.

Our platform's membrane-free design enables dynamic, quantitative, and label-free "liquid biopsies" of targeted brain regions by directly sampling ISF from distinct neural nodes and processing the sample using LC-MS/MS analytical techniques. The micro-invasive probes' spatial footprints are significantly smaller than traditional probes used for chemical sampling, such as microdialysis probes, which results in both increased spatial resolution and reduced inflammation of the surrounding tissue (*23*, *37*–*39*). Conducting push-pull perfusion through these single-lumen probes, with negligible dead volume and low-flow control, is enabled by the unique design of our bidirectional nanopump and cannot be accomplished with other previously designed or commercially available platforms. Acute samples of ISF obtained using our membrane-free device demonstrate the ability to detect large proteins that cannot be sampled using membrane-based techniques. Leaving the probe chronically implanted and plugging in the nanopump when required could also enable longitudinal sampling from a single neural node in the future.

The nanopump platform is able to extract meaningful biochemical information from ISF samples <1.5 µl in volume with the capability of readily tuning temporal resolution and could provide unprecedented insight into the composition of ISF in vivo. This platform could be used in the future to generate new fundamental knowledge of biomarker expression levels in well-established animal models of human disease. This has the potential to enable more accurate diagnosis of debilitating human neurological disorders. It could also be used to help identify new biochemical targets for investigational neurological therapies. The nanofluidic sampling platform could help address the critical technical challenge limiting the ability to measure the complete neurochemical connectome. We hope that it will be used to deepen the neuroscientific understanding of the onset, progression, and treatment of neural disease.

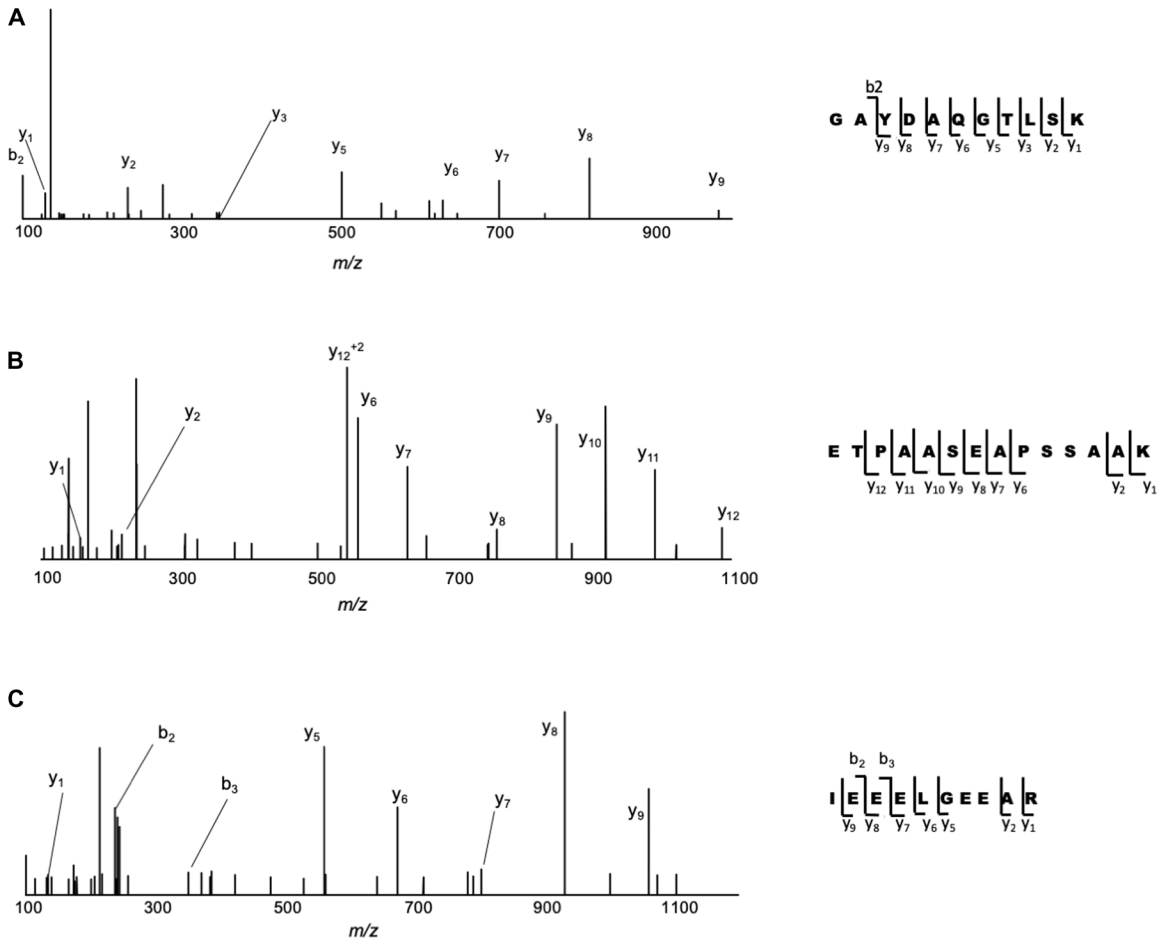

Fig. 5. Biochemical characterization of in vivo samples of neural ISF. (**A**) MS/MS spectrum identifying MBP in in vivo sample. (**B**) MS/MS spectrum identifying BASP-1 in in vivo sample. (**C**) MS/MS spectrum identifying γ-enolase in in vivo sample. Fragment ions identified in the MS/MS spectrum are labeled, with b-type fragment ions containing the N terminus and y-type fragment ions containing the C terminus.

METHODS

Pump design and characterization

The functional unit of the pump consists of two basic components: SEBS tubing that can interface with implantable microprobes and heat-sensitive shape memory alloy actuator wires. Tubing extracted from an iPrecio implantable pump (1 mm outer diameter, 500 μm inner diameter) was used for initial experiments, and a custom-manufactured tubing (Apollo Medical Extrusion Technologies) of dimensions 1 mm outer diameter and 100 μm inner diameter was used for in vitro, ex vivo, and in vivo characterization experiments. Wrapped around the tubing are four wires composed of the shape memory material nickel titanium alloy, nitinol (Flexinol, RobotShop). Wires of 37, 50, and 100 μm diameter were used, and all underwent a transition from a martensite phase to an austenite phase at 70°C. Current passed through the wire drives ohmic heating as a result of the alloy's high electrical resistance, resulting in physical contraction of the wire (up to 5% of original length) that displaces fluid within the SEBS tube. The current required to heat the wire and the time required to cool the wire are dependent on wire diameter and have been well characterized by the manufacturer. Wire displacement was monitored and recorded with a light microscope and processed via ImageJ software (National Institutes of Health) (*40*).

Borosilicate capillaries (outer diameter of 60 to 170 μm, inner diameter of 20 to 100 μm, VitroCom Inc.) were inserted within the SEBS tubing and sealed in place using an ultraviolet light-curable epoxy (Loctite 4305, Henkel Corp). For designs that incorporated removable connectors, capillaries were sealed in a PEEK tubing (1.59 mm outer diameter, 250 μm inner diameter, IDEX Health & Science), and a 30G needle (Atlantic Medical Supply) was press fit into both the PEEK and the SEBS tubing. Fluid flow through the tubing and probe is driven by sequential contraction of the nitinol wires in series, with the number and pre-tension of actuator wires, time heated, time cooled, and overlap between wires serving as tunable design parameters. Flow control algorithms were ranked on the basis of flow efficiency, with codes that minimized backflow preferred. The benchtop control electronics were formatted into a custom-manufactured printed circuit board (Advanced Circuits) controlled by an Arduino Uno and powered by 9-V batteries (Energizer L522) for the handheld miniaturized version of the pump. All functional units of the pump were enclosed within a custom three-dimensional–printed casing.

Flow within the SEBS tubing was monitored and recorded with a light microscope and processed via ImageJ software (National Institutes of Health) (*40*). The fluid meniscus was tracked over time,

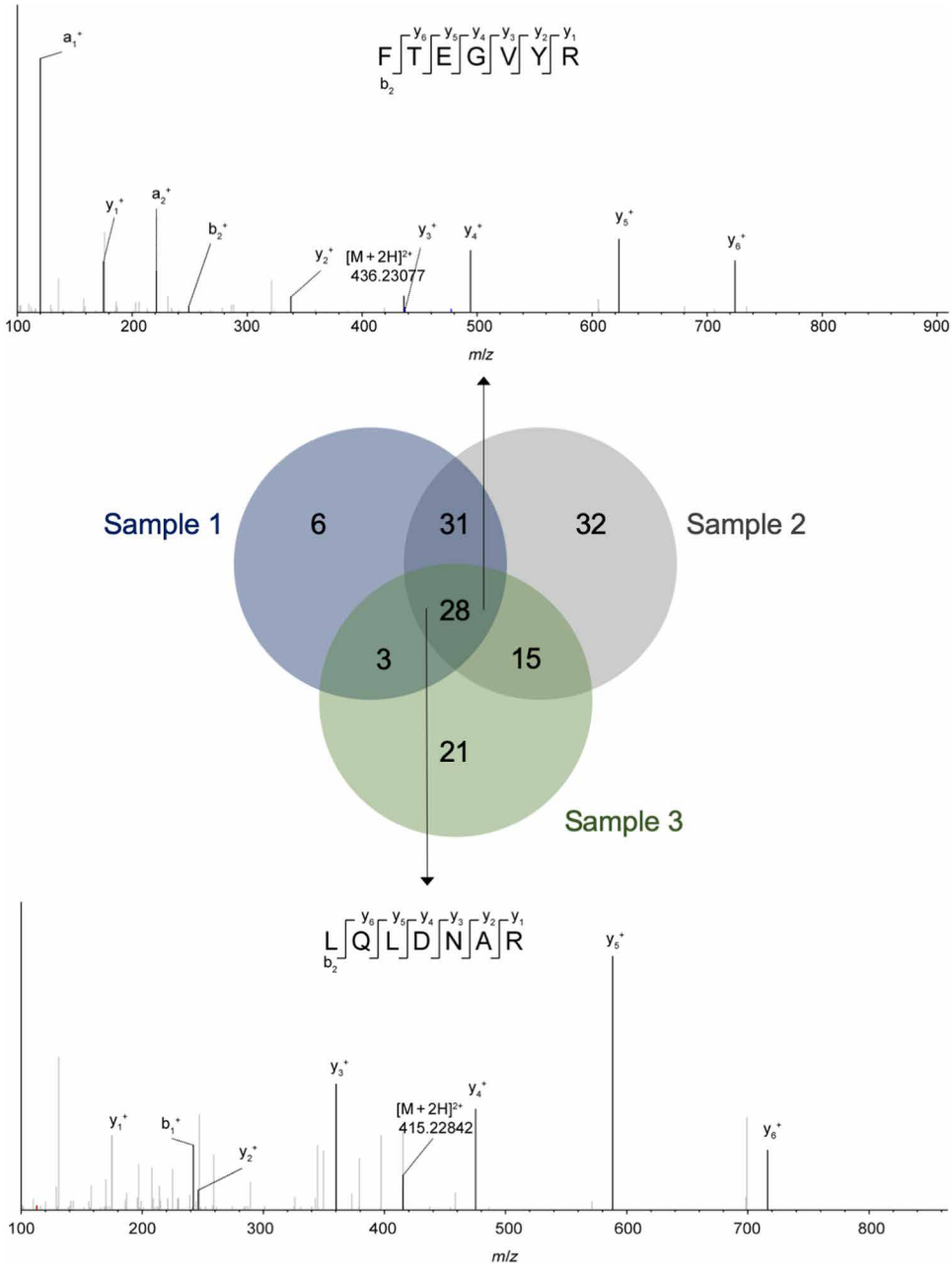

Fig. 6. Comparing biochemical profiles of in vivo samples of neural ISF. Middle: Venn diagram displaying the number of identified proteins in each of three in vivo samples from rat substantia nigra extracted using the nanopump. **Top**: MS/MS spectrum identifying transthyretin, found in all in vivo samples. **Bottom**: MS/MS spectrum identifying kinesin-like protein 15, found in all in vivo samples. Fragment ions identified in the MS/MS spectrum are labeled, with b-type fragment ions containing the N terminus and y-type fragment ions containing the C terminus. $[M + 2H]^{2+}$ denotes precursor ion.

and the known geometry of the tubing inner lumen was used to calculate fluid volume displaced as a function of time. In vitro tests in preparation for ex vivo and in vivo studies were conducted in agarose gel brain phantoms, prepared by mixing agarose (MilliporeSigma) with deionized (DI) water at a concentration of 0.6% by weight at 80°C until a clear mixture was formed. Gels were stored at 4°C when not in use.

Ex vivo and in vivo surgeries and characterization

Sprague-Dawley female rats were purchased from the Charles River Laboratories and maintained under 12-hour light/dark cycles. For ex vivo experiments, animals were euthanized using carbon dioxide asphyxiation. Brains were extracted immediately following sacrifice and used in infusion and sampling trails. Infusate was composed of either aCSF or Trypan blue for examination via LC-MS/MS or histology, respectively. aCSF was made in-house following protocols developed in the Graybiel laboratory and contains 128 mM NaCl, 4 mM KCl, 1.7 mM $CaCl_2$, 2.0 mM $MgCl_2$, 2.0 mM sodium phosphate buffer, 0.8 mM NaH_2PO_4, and 0.1 mM glucose in DI water. Solution was titrated until a pH of 7.4 was met and sterilized using 0.2-μm syringe filters (nylon membrane, Pall Corporation). Trypan

blue (0.4%; Sigma-Aldrich) was infused to visualize delivery to ex vivo tissue. Following infusion, brains were submerged in 10% formic acid (VWR) for 72 hours. Brains were then moved to increasing sucrose concentrations (Amresco Inc.). Tissue samples began immersion in 15% sucrose and were moved to 25% sucrose after 24 hours and left in 25% sucrose solution until they sank to the bottom of the container. The brain was then embedded in an optimal cutting temperature embedding medium (Sakura Finetek Inc.) and frozen via liquid nitrogen bath. Horizontal slices (15 μm) were obtained using a Leica CM1900 cryostat (Leica Biosystems Inc.), beginning on the dorsal surface descending the length of the tissue block. Slides were stored at −80°C until images could be taken using brightfield microscopy (EVOS Fl auto). Fluorescent dye infusion experiments were performed using the IVIS imaging system (PerkinElmer Inc.). Genhance 750 (0.05 mg/μl in 10× phosphate-buffered saline; PerkinElmer Inc.) was loaded into the sampling platform and infused into ex vivo brains or brain segments to demonstrate fluidic delivery into tissue. For static infusions, whole Sprague-Dawley brains were used with one infusion per hemisphere, and images were acquired for 2 s. In dynamic infusions, brain segments were used, and images were acquired every 6 s for a 60-s infusion.

Animals were anesthetized by inhalation of 3% isoflurane and maintained on 1 to 2% isoflurane throughout surgery for in vivo studies. Following anesthesia, animals were shaved and placed in a stereotaxic frame (Stoelting Co.). The shaved area was disinfected with alternating betadine and 70% ethanol swabs. Briefly, animals underwent a bilateral craniotomy. A midline incision was made to expose the skull. Two bilateral burr holes were made using a dental drill with a 1-mm drill bit (Meisinger GmbH) 5 mm posteriorly to bregma and 2 mm lateral to midline. The borosilicate capillary directly interfaced with the nanopump was lowered 8 mm from the brain surface, targeting the substantia nigra (SN), based on the *Paxinos and Watson Rat Brain Atlas*. Samples were withdrawn for 20 min following a 10-min infusion of sterile aCSF bilaterally. Animals were euthanized using carbon dioxide asphyxiation. All animal protocols were approved by the Massachusetts Institute of Technology Committee for Animal Care.

Sample storage and analysis

Samples obtained from in vivo and ex vivo sampling trials were stored in polypropylene microcentrifuge tubes (0.2 ml; VWR). Samples derived from ex vivo studies were immediately stored at −80°C. Samples taken during in vivo surgeries were stored in solid carbon dioxide until transferred to long-term storage at −80°C. Samples were processed within 1 week of storage.

Samples were thawed and denatured using 1% SDS (Sigma-Aldrich, 4509) for 1 hour at 95°C in preparation for analysis via LC-MS/MS. Acetonitrile (215 μl; Sigma-Aldrich, 34998) was added to each sample after cooling, and SDS was removed by a single-pot solid-phase–enhanced sample preparation (SP3) (GE Healthcare, 45152105050250 and Thermo Fisher Scientific, 65152105050250. Ten microliters of washed and equilibrated SP3 beads was added to each sample and incubated for 8 min. Supernatant was removed, and beads were rinsed three times with 100 μl of 80% acetonitrile. Residual acetonitrile was evaporated, and overnight on-bead proteolytic digestion was performed with trypsin (Promega, V5113) in 50 mM Hepes buffer (pH 8.5; Sigma-Aldrich, H3375). Sample was transferred to a fresh 1.5-ml tube and dried until a 10 μl of final volume was reached. One microliter of 10% acetic acid was added to the solution, and it was loaded onto a precolumn where it was washed with 0.1% acetic acid for 15 min before beginning analysis.

Peptide separation was carried out on an Agilent 1260 (Agilent Technologies) coupled to an Orbitrap Q-Exactive Plus (Thermo Fisher Scientific) for LC-MS/MS of trypsinized proteins. Peptides were loaded onto an analytical column with an integrated electrospray tip (1- to 2-μm orifice) following the wash step. Peptides were eluted with 70% acetonitrile in 0.2 M acetic acid (solvent B) in the following gradients: 0 to 30% solvent B in 8 min, 30 to 60% in 10 min, 60 to 100% in 5 min, and 100% for 5 min, before equilibrating back to solvent A. The flow was split to approximately 20 nl/min. The MS was operated in positive ion mode with a spray voltage of 2 kV and heated capillary temperature of 250°C. MS data were obtained in data-dependent acquisition mode. Full scans (MS1) were acquired in the mass/charge ratio (m/z) range of 350 to 2000 at a resolution of 70,000 (at m/z 200), with AGC (automatic gain control) target 3E6 and a maximum injection time of 50 ms. The top 15 most intense precursor ions were selected and isolated with an isolation width of 0.4 m/z and dynamic exclusion set to 20 s. Selected ions were HCD (higher-energy collisional dissociation) fragmented at normalized collision energy (NCE) 29 after accumulating to target value 1E5 with a maximum injection time of 350 ms. MS/MS acquisition was performed at a resolution of 35,000.

Raw mass spectral data files were processed via Proteome Discoverer version 2.2 (Thermo Fisher Scientific) and referenced against the Rat SwissProt database using Mascot version 2.4 (Matrix Science). Mascot is a probability-based algorithm that assesses the probability of an MS/MS spectrum matching to a given peptide from a database (*41*). MS/MS spectra were matched with an initial mass tolerance of 10 parts per million on precursor masses and 20 mmu (milli mass units) for fragment ions. Peptide spectrum matches for global proteomics data were filtered by Mascot score (≥30), and peptide assignments were confirmed by manual validation.

Collection and analysis for microdialysis nanopump comparison

Stock solutions of bovine hemoglobin (10 mg/15 ml; MilliporeSigma), MBP (2.87 mg/15 ml; MilliporeSigma), and 10 pmol of substance P (Abcam) were made up in DI water. Each was sampled using either nanopump or microdialysis. For microdialysis, a 20-kDa cutoff CMA 12 probe (Harvard Apparatus) was used. DI water was perfused at a rate of 1 μl/min into aliquots of hemoglobin, MBP, or substance P. Dialysate was collected in 30-min fractions into polypropylene vials. For nanopump samples, DI water was infused into stock solution for 10 min at a rate of 100 nl/min and withdrawn at a rate of 60 nl/min for 20 min into polypropylene vials.

Hemoglobin and MBP samples were analyzed via a NanoDrop Spectrophotometer ND-1000. The absorbance at 280 nm of either the nanopump- or microdialysis-derived samples was compared to an unsampled stock solution.

Relative concentration of substance P in either the unsampled stock solution or sampled via the nanopump or microdialysis device was analyzed by a nanospray LC-MS/MS (as previously described). Briefly, the collected samples were diluted 10-fold into a solution consisting of 0.1% acetic acid with 7 nM angiotensin as a loading control. One microliter of this final solution was loaded onto a custom analytical nano-LC column with an integrated electrospray ionization emitter tip. Peptides were eluted with 70% acetonitrile in 0.2 M acetic acid (solvent B) in a gradient going from 0 to 100%

solvent B in 8 min. The MS was operated in positive ion mode with a spray voltage of 2 kV and heated capillary temperature of 250°C. MS data were obtained in data-dependent acquisition mode. Full scans (MS1) were acquired in the *m/z* range of 350 to 1500 at a resolution of 70,000 (at *m/z* 200), with AGC target 1E6 and a maximum injection time of 150 ms. The top 15 most intense precursor ions were selected and isolated with an isolation width of 0.4 *m/z* and dynamic exclusion set to 10 s. Selected ions were HCD fragmented at NCE 28 after accumulating to target value 1E5, with a maximum injection time of 150 ms. MS/MS acquisition was performed at a resolution of 35,000.

SUPPLEMENTARY MATERIALS

Supplementary material for this article is available at http://advances.sciencemag.org/cgi/content/full/6/39/eabb0657/DC1

View/request a protocol for this paper from *Bio-protocol*.

REFERENCES AND NOTES

1. A. M. Andrews, Why monitor molecules in neuroscience? *ACS Chem. Neurosci.* **8**, 211–212 (2017).
2. E. V. Romanova, J. T. Aerts, C. A. Croushore, J. V. Sweedler, Small-volume analysis of cell–cell signaling molecules in the brain. *Neuropsychopharmacology* **39**, 50–64 (2014).
3. C. Dagdeviren, K. B. Ramadi, P. Joe, K. Spencer, H. N. Schwerdt, H. Shimazu, S. Delcasso, K.-i. Amemori, C. Nunez-lopez, A. M. Graybiel, M. J. Cima, R. Langer, Miniaturized neural system for chronic, local intracerebral drug delivery. *Sci. Transl. Med.* **10**, eaan2742 (2018).
4. H. N. Schwerdt, H. Shimazu, K.-i. Amemori, S. Amemori, P. L. Tierney, D. J. Gibson, S. Hong, T. Yoshida, R. Langer, M. J. Cima, A. M. Graybiel, Long-term dopamine neurochemical monitoring in primates. *Proc. Natl. Acad. Sci. U.S.A.* **114**, 13260–13265 (2017).
5. D. Scaini, L. Ballerini, Nanomaterials at the neural interface. *Curr. Opin. Neurobiol.* **50**, 50–55 (2018).
6. H. N. Schwerdt, E. Zhang, M. J. Kim, T. Yoshida, L. Stanwicks, S. Amemori, H. E. Dagdeviren, R. Langer, M. J. Cima, A. M. Graybiel, Cellular-scale probes enable stable chronic subsecond monitoring of dopamine neurochemicals in a rodent model. *Commun. Biol.* **1**, 144 (2018).
7. H. R. Noori, J. Schöttler, M. Ercsey-Ravasz, A. Cosa-Linan, M. Varga, Z. Toroczkai, R. Spanagel, A multiscale cerebral neurochemical connectome of the rat brain. *PLOS Biol.* **15**, e2002612 (2017).
8. V. I. Chefer, A. C. Thompson, A. Zapata, T. S. Shippenberg, Overview of brain microdialysis. *Curr. Protoc. Neurosci.* **47**, 7.1.1–7.1.28 (2009).
9. N. Nakatsuka, K.-A. Yang, J. M. Abendroth, K. M. Cheung, X. Xu, H. Yang, C. Zhao, B. Zhu, Y. S. Rim, Y. Yang, P. S. Weiss, M. N. Stojanović, A. M. Andrews, Aptamer-field-effect transistors overcome Debye length limitations for small-molecule sensing. *Science* **362**, 319–324 (2018).
10. Q.-T. Nguyen, L. F. Schroeder, M. Mank, A. Muller, P. Taylor, O. Griesbeck, D. Kleinfeld, An in vivo biosensor for neurotransmitter release and in situ receptor activity. *Nat. Neurosci.* **13**, 127–132 (2010).
11. D. C. Castro, M. R. Bruchas, A motivational and neuropeptidergic hub: Anatomical and functional diversity within the *Nucleus accumbens* shell. *Neuron* **102**, 529–552 (2019).
12. J. P. H. Burbach, What are neuropeptides? *Methods Mol. Biol.* **789**, 1–36 (2011).
13. A. N. van den Pol, Neuropeptide transmission in brain circuits. *Neuron* **76**, 98–115 (2012).
14. T. Hökfelt, T. Bartfai, F. Bloom, Neuropeptides: Opportunities for drug discovery. *Lancet Neurol.* **2**, 463–472 (2003).
15. E. Anderzhanova, C. T. Wotjak, Brain microdialysis and its applications in experimental neurochemistry. *Cell Tissue Res.* **354**, 27–39 (2013).
16. A. S. Darvesh, R. T. Carroll, W. J. Geldenhuys, G. A. Gudelsky, J. Klein, C. K. Meshul, C. J. Van der Schyf, In vivo brain microdialysis: Advances in neuropsychopharmacology and drug discovery. *Expert Opin. Drug Discov.* **6**, 109–127 (2011).
17. Q. Li, J.-K. Zubieta, R. T. Kennedy, Practical aspects of in vivo detection of neuropeptides by microdialysis coupled off-line to capillary LC with multistage MS. *Anal. Chem.* **81**, 2242–2250 (2009).
18. S. Takeda, N. Sato, K. Ikimura, H. Nishino, H. Rakugi, R. Morishita, Novel microdialysis method to assess neuropeptides and large molecules in free-moving mouse. *Neuroscience* **186**, 110–119 (2011).
19. K. M. Kendrick, Microdialysis measurement of in vivo neuropeptide release. *J. Neurosci. Methods* **34**, 35–46 (1990).
20. S. Koniusz, A. Andrzejewska, M. Muraca, A. K. Srivastava, M. Janowski, B. Lukomska, Extracellular vesicles in physiology, pathology, and therapy of the immune and central nervous system, with focus on extracellular vesicles derived from mesenchymal stem cells as therapeutic tools. *Front. Cell. Neurosci.* **10**, 109 (2016).
21. W. H. Lee, T. Ngernsutivorakul, O. S. Mabrouk, J.-M. T. Wong, C. E. Dugan, S. S. Pappas, H. J. Yoon, R. T. Kennedy, Microfabrication and in vivo performance of a microdialysis probe with embedded membrane. *Anal. Chem.* **88**, 1230–1237 (2016).
22. K. C. Spencer, J. C. Sy, K. B. Ramadi, A. M. Graybiel, R. Langer, M. J. Cima, Characterization of mechanically matched hydrogel coatings to improve the biocompatibility of neural implants. *Sci. Rep.* **7**, 1952 (2017).
23. M. J. Cotler, E. B. Rousseau, K. B. Ramadi, J. Fang, A. M. Graybiel, R. Langer, M. J. Cima, Steerable microinvasive probes for localized delivery to deep tissue. *Small* **15**, 1901459 (2019).
24. K. B. Ramadi, C. Dagdeviren, K. C. Spencer, P. Joe, M. Cotler, E. Rousseau, C. Nunez-Lopez, A. M. Graybiel, R. Langer, M. J. Cima, Focal, remote-controlled, chronic chemical modulation of brain microstructures. *Proc. Natl. Acad. Sci. U.S.A.* **115**, 7254–7259 (2018).
25. N. A. Cellar, S. T. Burns, J.-C. Meiners, H. Chen, R. T. Kennedy, Microfluidic chip for low-flow push-pull perfusion sampling in vivo with on-line analysis of amino acids. *Anal. Chem.* **77**, 7067–7073 (2005).
26. T. R. Slaney, J. Nie, N. D. Hershey, P. K. Thwar, J. Linderman, M. A. Burns, R. T. Kennedy, Push-pull perfusion sampling with segmented flow for high temporal and spatial resolution in vivo chemical monitoring. *Anal. Chem.* **83**, 5207–5213 (2011).
27. A. K. Au, H. Lai, B. R. Utela, A. Folch, Microvalves and micropumps for BioMEMS. *Micromachines* **2**, 179–220 (2011).
28. M. J. Cima, Microsystem technologies for medical applications. *Annu. Rev. Chem. Biomol. Eng.* **2**, 355–378 (2011).
29. N. Ludvig, G. Medveczky, R. Rizzolo, H. M. Tang, S. L. Baptiste, W. K. Doyle, O. Devinsky, C. Carlson, J. A. French, J. G. Kral, J. Charchaflieh, R. I. Kuzniecky, An implantable triple-function device for local drug delivery, cerebrospinal fluid removal and EEG recording in the cranial subdural/subarachnoid space of primates. *J. Neurosci. Methods* **203**, 275–283 (2012).
30. J. Fong, Z. Xiao, K. Takahata, Wireless implantable chip with integrated nitinol-based pump for radio-controlled local drug delivery. *Lab Chip* **15**, 1050–1058 (2015).
31. K. J. B. Lamers, P. Vos, M. M. Verbeek, F. Rosmalen, W. J. A. van Geel, B. G. M. van Engelen, Protein S-100B, neuron-specific enolase (NSE), myelin basic protein (MBP) and glial fibrillary acidic protein (GFAP) in cerebrospinal fluid (CSF) and blood of neurological patients. *Brain Res. Bull.* **61**, 261–264 (2003).
32. J.-P. Noben, D. Dumont, N. Kwasnikowska, P. Verhaert, V. Somers, R. Hupperts, P. Stinissen, J. Robben, Lumbar cerebrospinal fluid proteome in multiple sclerosis: Characterization by ultrafiltration, liquid chromatography, and mass spectrometry. *J. Proteome Res.* **5**, 1647–1657 (2006).
33. J. A. Hamilton, M. D. Benson, Transthyretin: A review from a structural perspective. *Cell. Mol. Life Sci.* **58**, 1491–1521 (2001).
34. D. W. Buster, D. H. Baird, W. Yu, J. M. Solowska, M. Chauvière, A. Mazurek, M. Kress, P. W. Baas, Expression of the mitotic kinesin Kif15 in postmitotic neurons: Implications for neuronal migration and development. *J. Neurocytol.* **32**, 79–96 (2003).
35. K. Sharma, S. Schmitt, C. G. Bergner, S. Tyanova, N. Kannaiyan, N. Manrique-Hoyos, K. Kongi, L. Cantuti, U.-K. Hanisch, M.-A. Philips, M. J. Rossner, M. Mann, M. Simons, Cell type- and brain region-resolved mouse brain proteome. *Nat. Neurosci.* **18**, 1819–1831 (2015).
36. R. R. Kitchen, J. S. Rozowsky, M. B. Gerstein, A. C. Nairn, Decoding neuroproteomics: Integrating the genome, translatome and functional anatomy. *Nat. Neurosci.* **17**, 1491–1499 (2014).
37. D. H. Szarowski, M. D. Andersen, S. Retterer, A. J. Spence, M. Isaacson, H. G. Craighead, J. N. Turner, W. Shain, Brain responses to micro-machined silicon devices. *Brain Res.* **983**, 23–35 (2003).
38. J. W. Salatino, K. A. Ludwig, T. D. Y. Kozai, E. K. Purcell, Glial responses to implanted electrodes in the brain. *Nat. Biomed. Eng.* **1**, 862–877 (2017).
39. L. Gällentoft, L. M. E. Pettersson, N. Danielsen, J. Schouenborg, C. N. Prinz, C. E. Linsmeier, Size-dependent long-term tissue response to biostable nanowires in the brain. *Biomaterials* **42**, 172–183 (2015).
40. J. Schindelin, I. Arganda-Carreras, E. Frise, V. Kaynig, M. Longair, T. Pietzsch, S. Preibisch, C. Rueden, S. Saalfeld, B. Schmid, J.-Y. Tinevez, D. J. White, V. Hartenstein, K. Eliceiri, P. Tomancak, A. Cardona, Fiji: An open-source platform for biological-image analysis. *Nat. Methods* **9**, 676–682 (2012).
41. D. N. Perkins, D. J. C. Pappin, D. M. Creasy, J. S. Cottrell, Probability-based protein identification by searching sequence databases using mass spectrometry data. *Electrophoresis* **20**, 3551–3567 (1999).

Acknowledgments: We thank T. Tamir, H. N. Schwerdt, K. Ramadi, G. Ekchian, T. Hua, H. Montague-Alamin, and M. Fahmi for technical discussions and help with this study.
Funding: This work was supported, in part, by the NIH (National Institute of Biomedical Imaging and Bioengineering grant R01 EB016101 to M.J.Ci., R.L., and A.M.G. and R01

EB027717-01A1 to M.J.Ci., R.L., and F.M.W.), the Center for Precision Cancer Medicine at MIT, and the Koch Institute Support (core) grant P30-CA14051 from the National Cancer Institute. R.R. was funded by the AAAS L'Oréal USA For Women in Science Fellowship and the NASEM Ford Foundation Fellowship. E.R. was funded by a NSF Graduate Research Fellowship (grant 2016220817). M.J.Co. was funded by a NSF Graduate Research Fellowship (grant 1122374). A.M.G. was funded by the NIH (National Institute of Mental Health grant R01 MH060379) and the Saks Kavanaugh Foundation. **Author contributions:** R.R., E.B.R., A.M.G., F.M.W., R.L., and M.J.Ci. designed the study. R.R., E.R., M.W., A.T., M.J.Co., J.K., A.A.L., and E.Z. performed experiments and helped write the Methods. R.R. and E.B.R. generated the manuscript and figures. All authors participated in manuscript and figure editing. **Competing interests:** M.J.Ci., R.L., and R.R. are inventors on a patent application related to this work filed by the Massachusetts Institute of Technology (no. 16/411,907; filed 14 November 2019). For a list of entities with which R.L. is involved, compensated or uncompensated, see: www.dropbox.com/s/yc3xqb5s8s94v7x/Rev%20Langer%20COI.pdf?dl=0. The other authors declare that they have no competing interests. **Data and materials availability:** All data needed to evaluate the conclusions in the paper are present in the paper and/or the Supplementary Materials. Additional data related to this paper may be requested from the authors.

Submitted 27 January 2020
Accepted 11 August 2020
Published 25 September 2020
10.1126/sciadv.abb0657

Citation: R. Raman, E. B. Rousseau, M. Wade, A. Tong, M. J. Cotler, J. Kuang, A. A. Lugo, E. Zhang, A. M. Graybiel, F. M. White, R. Langer, M. J. Cima, Platform for micro-invasive membrane-free biochemical sampling of brain interstitial fluid. *Sci. Adv.* **6**, eabb0657 (2020).

Science Advances

Platform for micro-invasive membrane-free biochemical sampling of brain interstitial fluid

Ritu Raman, Erin B. Rousseau, Michael Wade, Allison Tong, Max J. Cotler, Jenevieve Kuang, Alejandro Aponte Lugo, Elizabeth Zhang, Ann M. Graybiel, Forest M. White, Robert Langer and Michael J. Cima

Sci Adv **6** (39), eabb0657.
DOI: 10.1126/sciadv.abb0657

Science Advances (ISSN 2375-2548) is published by the American Association for the Advancement of Science, 1200 New York Avenue NW, Washington, DC 20005. The title *Science Advances* is a registered trademark of AAAS.